

DESIGN AND REALIZATION OF CIRCULAR CONTOURLET TRANSFORM

Dr. Jassim M. Abdul-Jabbar* and Hala N. Fathee**

* Ph. D in Elect. Eng., Dept. of Computer Eng., College of Eng., University of Mosul, Iraq

** M. Sc. in Computer Science, Dept. of Sport Science, College of Sport Educ., University of Mosul, Iraq.

Abstract

In this paper, circular contourlet transform (CCT) is proposed, designed and realized. As in the classical contourlet transform (CT), a double filter bank structure is also considered in this work but in different manners. A circularly-decomposed filter bank is first used to capture the points of discontinuities in the image edges, and then followed by a directional filter bank to obtain smoothed contours. The resulting CCT contains a critically sampled filter bank that decomposes images into any power of two's number of directional subbands at multiple scales. The designed CCT is realized by 2-D lattice allpass sections with separable and non-separable 2-D functions of z_1 and z_2 . The resulting structure preserves both modularity and regularity properties which are suitable for VLSI implementations. Objectively, the performances of the realized CCT are tested and proved to be better than the classical CT in detail image preservation. The resulting subband images also indicate the superiority of the proposed CCT.

Keywords: Circular contourlet transform, Contourlet transform, Laplacian pyramid, Directional filter bank, 2-D lattice allpass sections, Multiresolution (multiscale & multidirection) analysis.

تصميم وتحقيق تحويل كونتورلت الدائري

هالة نافع فتحي
كلية التربية الرياضية - فرع العلوم الرياضية
جامعة الموصل - العراق

د. جاسم محمد عبد الجبار
كلية الهندسة - قسم هندسة الحاسبات
جامعة الموصل - العراق

المستخلص

في هذا البحث تم اقتراح و تصميم وتحقيق تحويل كونتورلت الدائري. وكما هو تحويل كونتورلت التقليدي فقد استخدمت هيكلية أجراف مرشحات مزدوجة أيضا هنا، ولكن بشكل مختلف حيث استعمل جرف مرشحات دائري التقسيم أولا لمسك نقاط عدم الاستمرارية في حافات الصورة ثم أتبع بجرف مرشح آخر من النوع الإتجاهي للحصول على منحنيات حافات ناعمة. إن التحويل الناتج من هذه الهيكلية هو تحول كونتورلت دائري يجزيء الصور الى حزم ترددية جزئية إتجاهية بأعداد ثنائية وبقياسات متعددة. لقد تم تحقيق هذا التحويل باستخدام مقاطع إمرار كلية متشابكة بدوال ذات بعدين قابلة للفصل وأخرى غير قابلة للفصل بالمتغيرين z_1 و z_2 . إن الهياكل الناتجة تتمتع بخاصيتي القياسية التركيبية والانتظام وهما مناسبتان للبناء بتقنية VLSI. لقد تم فحص الأداء الموضوعي لتحويل كونتورلت الدائري ومقارنته ومع أداء تحويل كونتورلت التقليدي وأثبت تفوقه عليه في الحفاظ على تفاصيل حافات الصورة. كما إن صور الحزم الفرعية الناتجة من التقنية المقترحة CCT تثبت جدواها.

I. INTRODUCTION

Although the wavelet transform (WT) is known to be a powerful tool in many signal and image processing applications such as compression, noise removal, image edge enhancement, and extraction; *wavelets* are not optimal in capturing the two-dimensional singularities found in images and often required in many segmentation and compression applications [1]-[3]. In particular, natural images consist of edges that are smooth curves which cannot be captured efficiently by the wavelet transform. Therefore, several new transforms are required for image signals.

The contourlet transform (CT) is one of the new geometrical image transforms, which can efficiently represent images containing contours and textures[4]-[6]. This transform uses a structure similar to that of curvelets [7]-[10], that is, a stage of subband decomposition followed by a directional transform. In the contourlet transform, a Laplacian pyramid (LP) is employed for the first stage, while directional filter banks (DFBs) are used in the angular decomposition stage. A comparison between the wavelet scheme and the contourlet shows the improved edge contours of the later [6],[11]. This is attributed to the grouping of nearby wavelet coefficients, since they are locally correlated due to the smoothness of the contours as shown in Fig. 1. Therefore, a sparse expansion for natural images can be obtained by first applying a multiscale transform, followed by a local directional transform to gather the nearby basis functions at the same scale into linear structures. In essence, a wavelet-like transform for edge detection, and then a local directional transform for contour segment detection are applied. The overall result is an image expansion using basic elements like contour segments, and thus are named contourlets and the process is called the contourlet transform (CT).

Circular split 2-D spectral schemes (circularly-decomposed frequency subspaces) are known to give better performance than rectangular-support or diamond-support schemes when it is desired to extract as low frequency information as possible in a 2-D low-pass filtering process. This also means that circular split schemes are preferred to extract as high frequency information as possible in a 2-D high-pass filtering process [12].

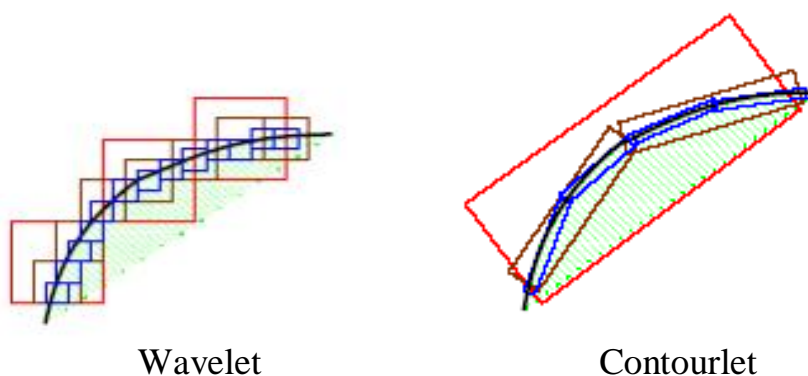


Fig. 1 The successive refinement by the two systems (wavelet and contourlet) near a smooth contour, which is shown as a thick curve separating two smooth regions.

In this paper, A circular contourlet transform (CCT) is proposed, designed and then efficiently realized. A double filter bank structure is also applied. Using circularly-decomposed filter bank, A circular split scheme (CSS) is first employed to capture the points of discontinuities, and then followed by a directional filter bank (DFB) to obtain

smoothed structures. The resulting CCT decomposes images into directional subbands at multiple scales and contains a critically sampled filter bank that decomposes images into any power of two's number of directions. The rest of this paper is organized as follows: The contourlet transform is described in section II. Section III contains the multiscale and multidirection analysis of such transform. In section IV, the proposed circular contourlet transform is formulated, designed and realized using 2-D lattice allpass sections with separable and non-separable 2-D functions of z_1 and z_2 (z_1 and z_2 are the 2-D complex spatial frequencies in the discrete spectral domain). The quantitative and qualitative performances of the realized CCT transform are examined and compared with those of the classical CT transform in section V. Finally, section VI concludes this paper.

II. THE CONTOURLET TRANSFORM

The contourlet transform consists of two major stages: the subband decomposition and the directional transform. At the first stage, LP is used to decompose the image into subbands, and then the second one is a DFB which is used to analyze each detail image. A flow graph of the CT is shown in Fig. 2. Example of the spectral split scheme achieved by such LP is shown in Fig. 3. 2-D filters may be employed in the realization of this stage. Example of the directionally-decomposed frequency split scheme achieved by such DFB is shown in Fig. 4. 2-D fan filters which serve as the building blocks of this DFB have wedge-shaped passband spectral regions [10] as in Fig. 4.

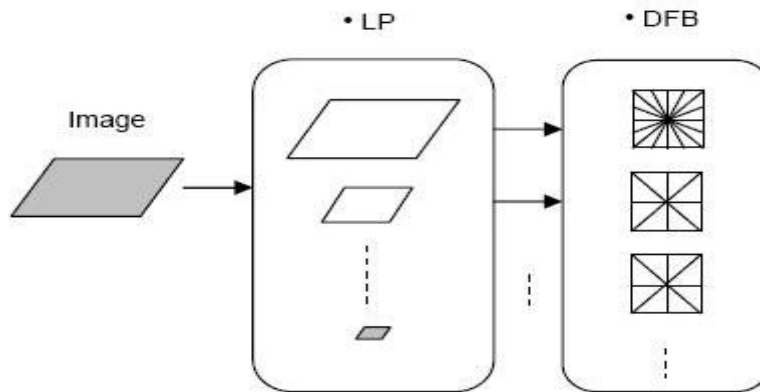


Fig. 2 A flow graph of the contourlet transform. The image is first decomposed into subbands by LP and then each detail image is analyzed by DFB.

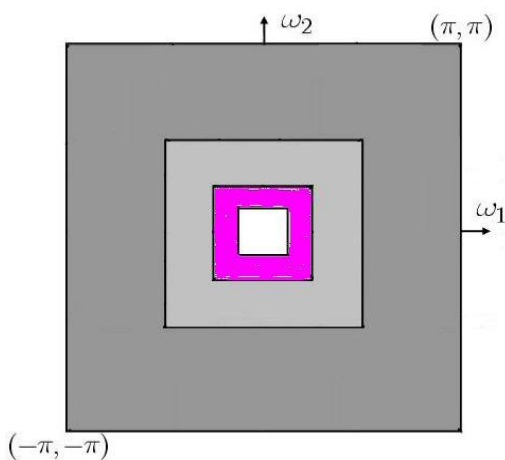


Fig. 3 The spectral split scheme of LP filter .

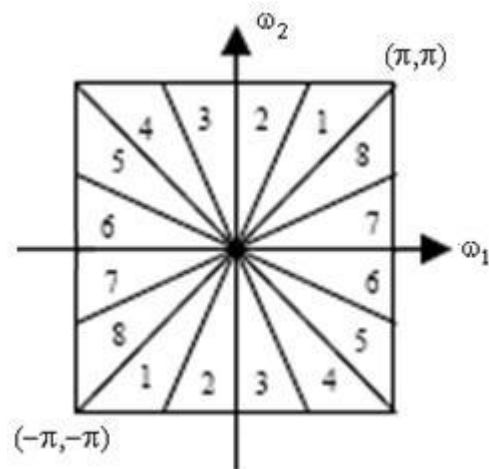


Fig. 4 An example of the directional bank frequency partitioning .

It is easily shown that these wedge-shaped regions correspond to directional components of the image [8], [9]. All 2-D filters employed are 2-D extensions of the 1-D filters previously designed to satisfy perfect / aliasing-free reconstruction constraints [12]. The resulting 2-D filter functions are nonseparable in z_1 & z_2 .

Since, the CT is formed precisely via a new multiresolution analysis framework that is similar to the link between wavelets and filter banks [1], the new elements in this framework are multidirection and its combination with multiscale.

With this insight, a double filter bank structure (see Fig. 5a) is used for obtaining sparse expansions for typical images having smooth contours [5], [6]. In this double filter bank, the LP (rectangular-support scheme) is first used to capture the points of discontinuities, and then followed by a DFB (directionally-decomposed split scheme) to link points of discontinuities into smooth curves [4]. The overall result is an image expansion using basic elements like contour segments, and thus are named contourlets. In particular, contourlets have elongated supports at various scales, directions, and aspect ratios. Thus allows contourlets to efficiently approximate a smooth contour at multiple resolutions just like the scheme shown in Fig. 5b. From frequency domain point of view, CT provides both multiscale and multidirectional decompositions.

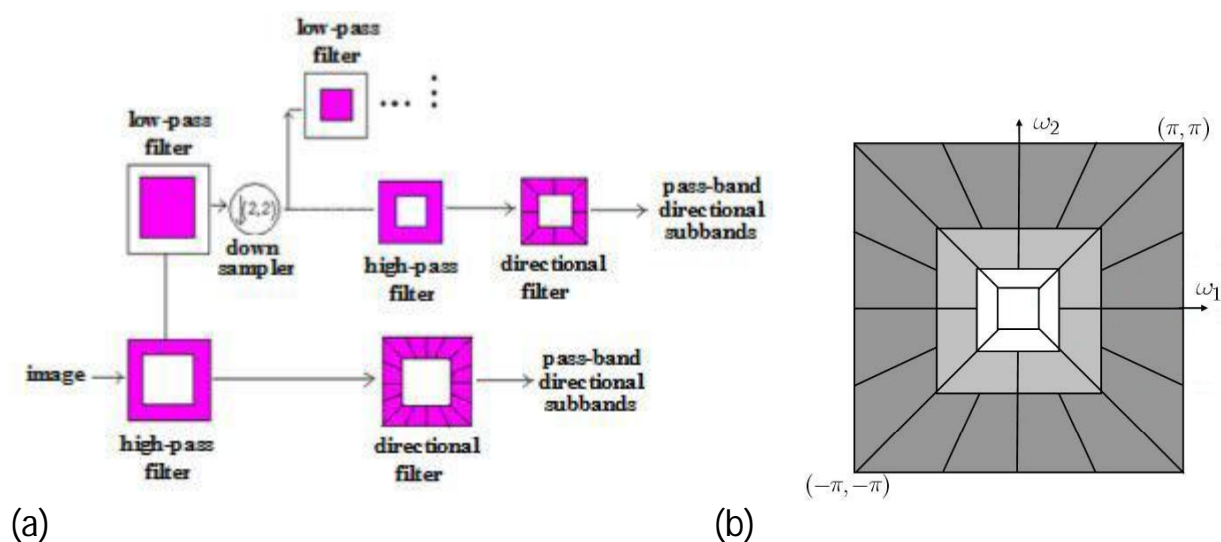


Fig. 5 (a) The contourlet filter bank: first, a multiscale decomposition into octave bands by LP is computed, and then a DFB is applied to each bandpass channel, (b) A typical contourlet frequency partition scheme.

III. MULTIREOLUTION ANALYSIS

In the followings and for simplicity, the case with orthogonal filters, which lead to tight frames will be considered only. The more general case with biorthogonal filters can be treated similarly. Multiresolution analysis is divided into the following two analysis:

A) Multiscale analysis

This is the multiresolution analysis for the LP, which is similar to the one for wavelets. Suppose that the LP in the contourlet filter bank uses orthogonal filters and down sampling by 2 in each dimension as shown in Fig. 6 (that means $M = \text{diag}(2,2) = \begin{bmatrix} 2 & 0 \\ 0 & 2 \end{bmatrix}$). Under certain

regularity conditions, the lowpass synthesis filter G in the iterated LP uniquely defines a unique scaling function $\phi(t) \in L_2(R^2)$ that satisfies the following two-scale equation [1], [2].

$$\sqrt{2}\phi(t) = 2 \sum_{n \in Z^2} g[n] \phi(2t - n). \quad (1)$$

where $g[n]$ is the impulse response of the lowpass synthesis filter G . Let

$$\phi_{j,n} = 2^{-j} \phi\left(\frac{t - 2^j n}{2^j}\right), \quad j \in Z, n \in Z^2. \quad (2)$$

Then the family $\{\phi_{j,n}\}_{n \in Z^2}$ is an orthonormal basis for an approximation subspace V_j at the scale 2^j . Furthermore, $\{V_j\}_{j \in Z}$ provides a sequence of multiresolution nested subspaces $\dots V_2 \subset V_1 \subset V_0 \subset V_{-1} \subset V_{-2} \dots$, where V_j is associated with a uniform grid of intervals $2^j \times 2^j$ that characterizes image approximation at scale 2^j . The difference images in the LP contain the details necessary to increase the resolution between two consecutive approximation subspaces. Therefore, the difference images live in a subspace W_j that is the orthogonal complement of V_j in V_{j-1} (see Fig. 7a), or

$$V_{j-1} = V_j \oplus W_j. \quad (3)$$

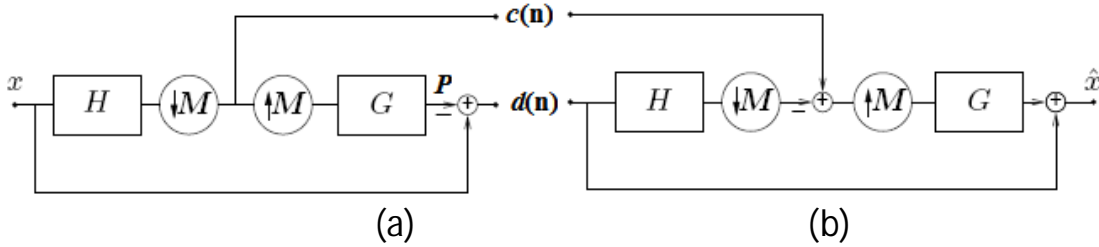


Fig. 6 LP scheme; (a) Analysis: Outputs are a coarse approximation $c(n)$ and a difference $d(n)$ between the original signal and the prediction P . The process can be iterated by decomposing the coarse version repeatedly, (b) Usual synthesis.

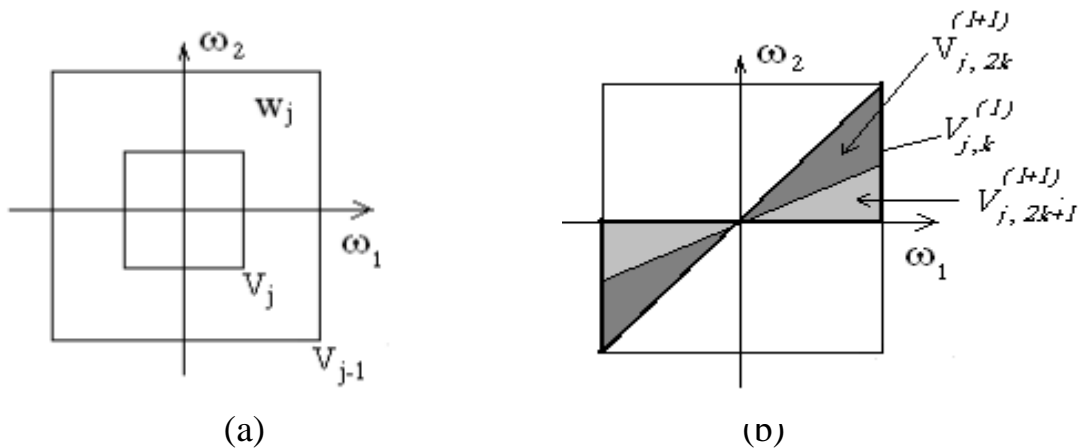


Fig. 7 (a) Multiresolution Analysis: scale, (b) Multiresolution Analysis: direction

It is believed that the LP can be considered as an oversampled filter bank where each polyphase component of the difference image $d[n]$ in Fig. 6, together with the coarse image

$c[n]$, comes from a separate filter bank channel with the same sampling matrix $M = \text{diag}(2,2)$. Let $F_i(z)$, $0 \leq i \leq 3$ be the synthesis filters for these polyphase components. These are highpass filters. As for wavelets, a continuous function $\psi^{(i)}(t)$, can be associate with each of these filters, where

$$\sqrt{2} \psi^{(i)}(t) = 2 \sum_{n \in \mathbb{Z}^2} f_i[n] \phi(2t - n). \quad (4)$$

where $f_i[n]$ is the impulse response of the highpass synthesis filter $F_i(z)$.

So, letting $\psi^{(i)}(t)$ in (4), be in the following form

$$\psi_{j,n}^{(i)}(t) = 2^{-j} \psi^{(i)}\left(\frac{t - 2^j n}{2^j}\right), \quad j \in \mathbb{Z}, n \in \mathbb{Z}^2 \quad (5)$$

Then, for scale 2^j , $\{\psi_{j,n}^{(i)}\}_{0 \leq i \leq 3, n \in \mathbb{Z}^2}$ is tight frame for W_j . For all scales, $\{\psi_{j,n}^{(i)}\}_{j \in \mathbb{Z}, 0 \leq i \leq 3, n \in \mathbb{Z}^2}$ is a tight frame for $L_2(\mathbb{R}^2)$. In both cases, the frame bounds are equal to 1. Since W_j is generated by four kernel functions (similar to multi-wavelets), in general it is not a shift-invariant subspace. Nevertheless, a shift-invariant subspace can be simulated by denoting

$$\mu_{j,2n+k_i}(t) = \psi_{j,n}^{(i)}(t), \quad 0 \leq i \leq 3, \quad (6)$$

where k_i are the coset representatives for down sampling by 2 in each dimension, *i.e.*,

$$k_0 = (0,0)^T, k_1 = (1,0)^T, k_2 = (0,1)^T, k_3 = (1,1)^T. \quad (7)$$

With this notation, the family $\{\mu_{j,n}\}_{n \in \mathbb{Z}^2}$ associated to a uniform grid of intervals $2^{j-1} \times 2^{j-1}$ on \mathbb{R}^2 provides a tight frame for W_j .

B) Multidirection Analysis

Using multirate identities [2], it is instructive to view an l -level tree-structured DFB equivalently as a 2^l parallel channel filter bank (as in Fig. 8) with equivalent analysis filters, synthesis filters and overall sampling matrices. In Fig. 8, the equivalent directional analysis filters are denoted as $E_k^{(l)}$, $0 \leq k \leq 2^l$, and the directional synthesis filters as $D_k^{(l)}$, $0 \leq k < 2^l$, which correspond to the subbands indexed as in Fig. 7. The corresponding overall sampling matrices S_k^l are proved to have the following diagonal forms [1]

$$S_k^{(l)} = \begin{cases} \begin{bmatrix} 2^{l-1} & 0 \\ 0 & 2 \end{bmatrix} & 0 \leq k < 2^{l-1}, \quad (\text{"near horizontal" direction}) \\ \begin{bmatrix} 2 & 0 \\ 0 & 2^{l-1} \end{bmatrix} & 2^{l-1} \leq k < 2^l \quad (\text{"near vertical" direction}) \end{cases} \quad (8)$$

which means sampling is separable. The two sets correspond to the *mostly horizontal* and *mostly vertical* set of directions, respectively. From the equivalent parallel view of the DFB, it can be seen that the family

$$\{d_k^{(l)}[n - S_k^{(l)}m]\}_{0 \leq k < 2^l, m \in \mathbb{Z}^2}, \quad (9)$$

obtained by translating the impulse responses of the equivalent synthesis filters $D_k^{(l)}$ over the sampling lattices by $S_k^{(l)}$, provides a *basis* for discrete signals in $L_2(\mathbb{Z}^2)$. This basis exhibits both directional and localization properties. In the iterated contourlet filter bank, the discrete basis (9) of the DFB can be regarded as a change of basis for the continuous-domain subspaces from the multiscale analysis of the previous LP stage. Suppose that the DFB in the contourlet filter bank utilizes orthogonal filters and when such DFB is applied to the difference image (detail) subspaces, then the resulting detail directional subspaces $W_{j,k}^{(l)}$ in the frequency domain will

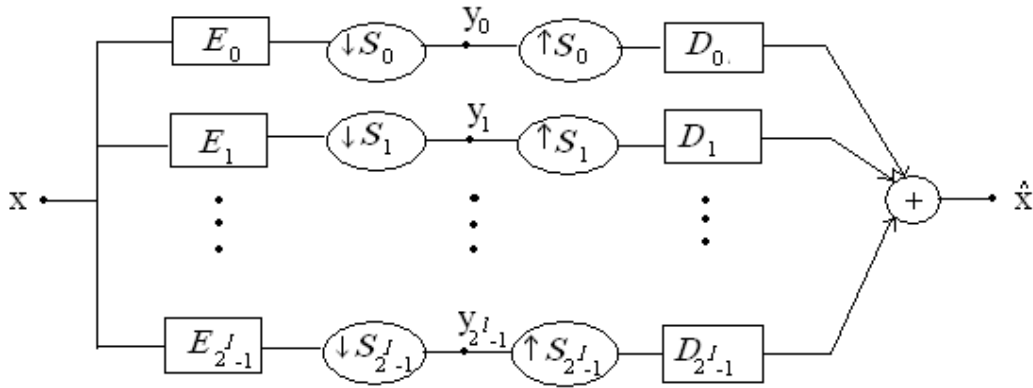


Fig. 8 The multichannel view of an l -level tree-structured DFB,

be as illustrated in Fig. 9. The indexes j , k , and n specify the scale, direction, and location, respectively. Note that the number of DFB decomposition levels l is different at different scales j , and is denoted by l_j . Recall that W_j is not a shift-invariant subspace. However, its subspaces $W_{j,k}^{(l)}$ are regenerative, since they are generated by a single function and its translations.

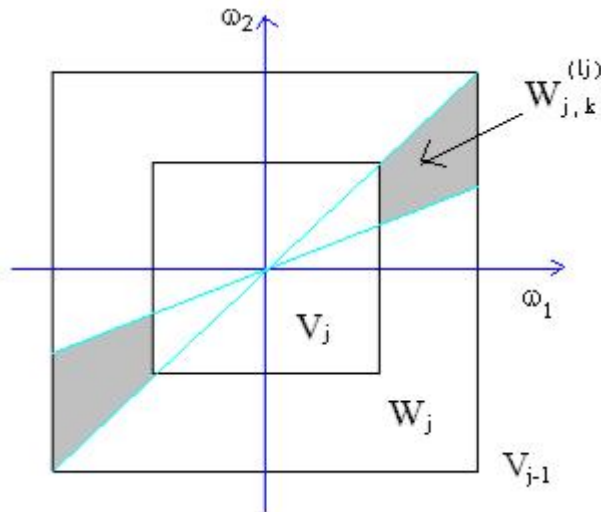


Fig. 9 Multiscale and multidirection subspaces generated by the transform which is illustrated on a 2-D spectrum decomposition .

For a contourlet filter bank, the following properties hold [11], [13]:

- (1) If both the LP and the DFB use perfect-reconstruction filters, then the discrete contourlet transform achieves perfect reconstruction, which means it provides a frame operator.
- (2) If both LP and the DFB use orthogonal filters, then the CT provides a tight frame with frame bounds equal to 1.
- (3) The discrete contourlet transform has a redundancy ratio that is less than 4/3.
- (4) Suppose an l_j -level DFB is applied at the pyramidal level j of the LP, then the basis images of the discrete contourlet transform (i.e. the equivalent filters of the contourlet filter bank) will have an essential support size of $width \approx C 2^j$ and $length \approx C 2^{j+l_j-2}$, where C is a constant.
- (5) Using FIR filter realizations, the computational complexity of the CT is $O(N)$ for N -pixel images.

IV. THE PROPOSED CIRCULAR CONTOURLET TRANSFORM (CCT)

A) Formulation and properties

The proposed circular contourlet is a cascade of a circular split scheme (CSS) and a DFB as shown in Fig. 10a. Such structure decomposes images into directional subbands at circular multiple scales. The DFB is a critically sampled filter bank that decomposes images into any power of two's number of directions. Due to this cascaded structure, the circular multiscale and directional decompositions are independent of each other. One can decompose each scale into any arbitrary power of two's number of orientations and different scales can be divided into different numbers of orientations. Fig. 10b also shows the proposed frequency division of the circular contourlet transform where three of the four scales are divided into two, four, and eight directional subbands from coarse to fine scales, respectively.

Figure 11 illustrates the subspace generation by CCT. In Fig. 11a, V_j is a subspace, defined on a uniform circular grid. The difference image (W_j subspace in the CSS) carries the details necessary to increase the resolution from V_j to V_{j-1} on an image approximation; index k runs to all 2^l directions. Figure 11b illustrates the subspace generation by the directional decomposition and the increase in the resolution from $V_{j,k}^{(1)}$ to $V_{j,2k}^{(1+1)}$ and $V_{j,2k+1}^{(1+1)}$ and $W_{j,2k}^{(1+1)}$ and $W_{j,2k+1}^{(1+1)}$, in Fig. 11c, are the resulting subspaces from the applications of the directional decomposition on the details subspace W_j in the CSS.

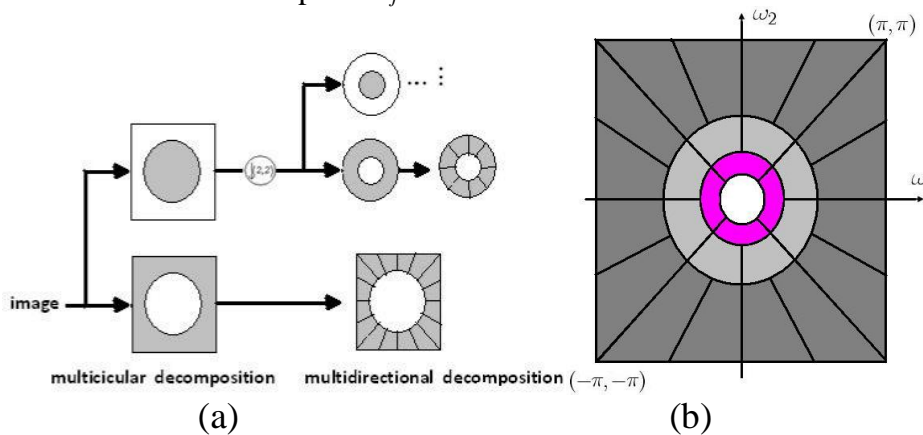


Fig. 10 (a) The proposed the discrete circular contourlet transform implementation.
 (b) Its frequency partition scheme.

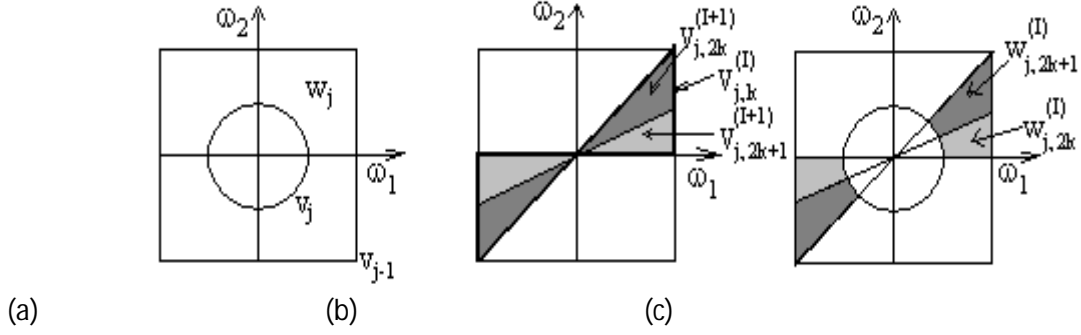


Fig. 11 Generation of subspaces by CCT; j subspace index; k direction; l all commands
 (a) CSS decomposition. (b) directional decomposition. (c) CCT subspaces.

B) Design and realization

The design of the circular split scheme (CSS) 2-D filters starts from the 1-D splitting orthogonal filters in Fig. 12a. In such figure and for perfect-reconstruction , it can be written as

$$h(z) \tilde{h}(z^{-1}) + g(z^{-1}) \tilde{g}(z) = 1 \quad (10)$$

where

$$\left. \begin{aligned} g(z) &= h(-z) \\ \tilde{h}(z) &= g(-z) = h(z) \\ \text{and} \\ \tilde{g}(z) &= h(-z) \end{aligned} \right\} \quad (11)$$

(10) can be evaluated on the unit circle ($z = e^{i\omega}$) as

$$\left| h(e^{i\omega}) \right|^2 + \left| h(e^{i\omega+\pi}) \right|^2 = 1 \quad (12)$$

It is clear, that condition (12) is met for all ω , even at $\omega = \pi/2$ and leads to a LP-HP power complementary filter pairs with perfect-reconstruction. It should be noted here that constraints (11) does not impose any phase conditions. Nevertheless, the approach will result in zero-phase properties of the total system. Condition (12) can easily be written in the following from:

$$\left| h(e^{i\omega}) \right|^2 + \left| g(e^{i\omega}) \right|^2 = 1 \quad , \text{for all } \omega \quad (13)$$

Keeping the condition (13) in mind, $h(z)$ and $g(z)$ can be expressed as the sum and difference of two all-pass sections, where

$$h(z) = \frac{1}{2} [a_0(z) + a_1(z)] \quad (14a)$$

and

$$g(z) = \frac{1}{2} [a_0(z) - a_1(z)] \quad (14b)$$

where $a_0(z)$ and $a_1(z)$ are stable all-pass functions.

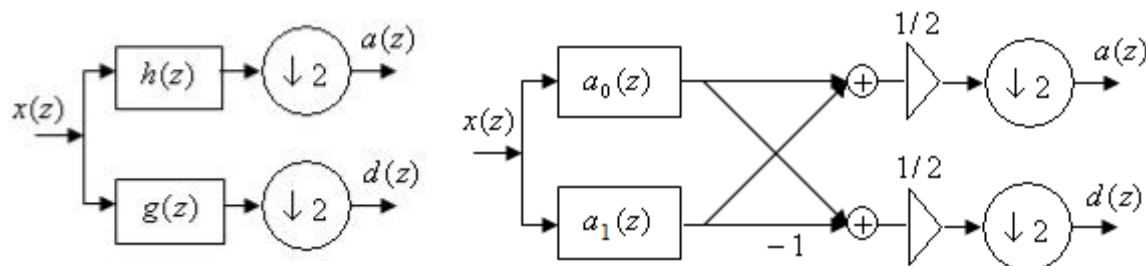


Fig. 12 (a) 1-D analysis bank, (b) Lattice all-pass equivalent filter bank.

The structure in Fig. 12b represents the lattice all-pass equivalence of the analysis bank of Fig. 12a which satisfy (14a&b). It should be noted that the lattice all-pass equivalent structure of the synthesis bank is identical to the 2-band analysis bank and can also be represented as the sum and difference of two all-pass sections. However, the design of the desired circular split scheme (CSS) 2-D filter bank is an extension of the 1-D filter bank via a suitable 1-D to 2-D transformation. It should be noted, here, that the circular decomposition scheme requires some nonlinear change of variables, such as [12]

$$z'_1 = f_1(z_1) f_2(z_2) \quad (15a)$$

and

$$z'_2 = f_1(z_1) f_2(z_2^{-1}) \quad (15b)$$

where

$$f_i(z_i) = \frac{z_i + \alpha_i}{1 + \alpha_i z_i} \quad \text{for } i = 1, 2 \quad (16)$$

with $\alpha_1 = \alpha_2$ for circular shape decomposition.

The choice of α_1 and α_2 values provides the appropriate bending for the supports to be look like circular shapes. On the other hand, the values of α_1 and α_2 are limited to

$$|\alpha_i| < 1 \quad \text{for } i = 1, 2. \quad (17)$$

to insure stability [12].

It should be noted that, (16) is nonlinear transformation called the digital spectral transformation (DST) [12], [13]. Due to this non-linearity, these variations of variables cannot be readily incorporated in the sampling rate alteration filters. Therefore, such changes can be incorporated in the analysis/synthesis filters themselves, resulting in 2-D all-pass sections which are nonseparable, although however they can be efficiently realized as will be shown in the following discussion:

The circularly-decomposed filter banks can be realized, using the same 1-D structure shown in Fig. 12a, but with $h(z)$ being transformed via the DST to $h(z_1, z_2)$ which can be formed as [12]

$$h(z_1, z_2) = h(z'_1) h(z'_2) h(f_1(z_1)) h(f_2(z_2)) \quad (18)$$

where z'_1 and z'_2 are as those given in (15a&b) and $f_i(z_i)$ is as given in (16).

It was proved previously in [14], that the application of this DST to linear-phase 1-D filter leads to 2-D filters which preserve the linear-phase characteristics approximately. Thus, it can be concluded that the application of this DST to the 1-D filter banks, in Fig. 12a, will lead to 2-D circular filter banks for perfect reconstruction of images. The equivalent filter

bank in Fig. 12b can be used. Since, it is realized in a lattice all-pass sections, then some saving in computation can be gained, while lattice structure will provide the system with a reduced sensitivity to finite word length of multiplier values [11].

The support of circularly-symmetric response of 2-D low-/high-pass splitting scheme is shown in Fig. 11a, the cutoff curve in this scheme is characterized by the circle $\omega_c = \pi/2$, where ω_c is the 2-D cutoff frequency in rad. The pass-band is described by the region $\left\{ \omega_1, \omega_2 : 0 \leq \sqrt{\omega_1^2 + \omega_2^2} \leq \omega_c \right\}$ while the stop-band is described by the region $\left\{ \omega_1, \omega_2 : \omega_c < \sqrt{\omega_1^2 + \omega_2^2} < \infty \right\}$.

The same 1-D structure shown in Fig. (3.3a) with $h(z)$ and $g(z)$ being 1-D filters chosen to be realized as Haar orthogonal filters [$h(z) = \frac{1}{\sqrt{2}} + \frac{1}{\sqrt{2}} z^{-1}$ and $g(z)$ is as given in (11)], while, their 2-D versions $h(z_1, z_2)$ and $g(z_1, z_2)$, used for the realization of the CSS scheme, are identical to that of (18). After designing and realizing this 2-band circular-split scheme, a second stage of DFB still have to be designed and realized. In such a stage, the design of the 2-D DFB will also start from the 1-D splitting filters in Fig. 12b with the two 1-D all-pass sections $a_0(z)$ and $a_1(z)$ being replaced by their 2-D counterparts. As in Fig. 13, a 3-level tree decomposition structure is used to serve for an 8-band directional decomposition. The Haar orthogonal filters are also utilized, here, and realized as a two 1-D all-pass sections in a lattice structure, with

$$a_0(z) = \sqrt{2} \tag{19a}$$

and

$$a_1(z) = \sqrt{2} z^{-1} \tag{19b}$$

The corresponding 2-D lattice all-pass sections in the first level of the tree structure of Fig.13 will yield a 2-band directional-decomposed split scheme. These sections can be derived as [11]

$$A_0(z'_1, z'_2) = a_0(\sqrt{-z_1 z_2}) a_0(\sqrt{-z_1 z_2^{-1}}) \tag{20a}$$

and

$$A_1(z'_1, z'_2) = a_1(\sqrt{-z_1 z_2}) a_1(\sqrt{-z_1 z_2^{-1}}) \tag{20b}$$

The transfer functions till the outputs of the first level of directional decomposition $DA_0(z_1, z_2)$ and $DA_1(z_1, z_2)$ can be written in matrix form as

$$\begin{bmatrix} DA_0(z_1, z_2) \\ DA_1(z_1, z_2) \end{bmatrix} = \frac{1}{2} \begin{bmatrix} 1 & 1 \\ 1 & -1 \end{bmatrix} \begin{bmatrix} A_0(z_1, z_2) \\ A_1(z_1, z_2) \end{bmatrix} \tag{21}$$

The resulting 2-band directionally-decomposed filter bank can be realized as in Fig. 12b, but with $a_0(z)$ and $a_1(z)$ being replaced by $A_0(z'_1, z'_2)$ and $A_1(z'_1, z'_2)$ given in (12a&b), respectively.

At the second level of the tree structure, a 4-band directional-decomposed split scheme is also formed as in Fig. 13. It is realized just like the previously mentioned Haar lattice all-pass structure with $a_0(z)$ and $a_1(z)$ being replaced by

$$B_i(z'_1, z'_2) = a_i(j, z_1) a_i(j, z_2) \quad \text{for } i = 0, 1. \quad (22)$$

The transfer functions till the outputs of the second level of directional decomposition $DA_0(z_1, z_2)$ and $DA_1(z_1, z_2)$ can be written as

$$DA'_i(z_1, z_2) = \frac{1}{4} [A_0(z_1, z_2) + A_1(z_1, z_2)] [B_0(z_1, z_2) \mp B_1(z_1, z_2)] \quad , \quad \text{for } i=0, 1. \quad (23a)$$

and

$$DA'_i(z_1, z_2) = \frac{1}{4} [A_0(z_1, z_2) - A_1(z_1, z_2)] [B_0(z_1, z_2) \mp B_1(z_1, z_2)] \quad , \quad \text{for } i=2, 3. \quad (23b)$$

The all-pass functions in third level of the tree structure of the directional decomposition stage (Fig.13) form the final requirement to accomplish an 8-band directional-decomposed split scheme. These functions are given by [11]

$$C_{ji}(z_1, z_2) = A_i(z_1, z_2) \quad , \quad \text{for } i = 0, 1 \quad (24)$$

$$\text{with } \left. \begin{array}{l} z_1 = z_1 z_2^{-2} \\ z_2 = z_1 \end{array} \right\}, \text{ for } j = 1, \quad \left. \begin{array}{l} z_1 = z_1^{-2} z_2 \\ z_2 = z_2 \end{array} \right\}, \text{ for } j = 2, \\ \left. \begin{array}{l} z_1 = z_1 \\ z_2 = z_1 z_2^2 \end{array} \right\}, \text{ for } j = 3, \text{ and } \left. \begin{array}{l} z_1 = z_2 \\ z_2 = z_1^2 z_2 \end{array} \right\}, \text{ for } j = 4.$$

Thus, the overall 8-band directionally-decomposed filter bank transfer functions are

$$\begin{aligned} DA_0''(z_1, z_2) &= \frac{1}{8} [A_0(z_1, z_2) + A_1(z_1, z_2)] [B_0(z_1, z_2) + B_1(z_1, z_2)] [C_{10}(z_1, z_2) + C_{11}(z_1, z_2)], \\ DA_1''(z_1, z_2) &= \frac{1}{8} [A_0(z_1, z_2) + A_1(z_1, z_2)] [B_0(z_1, z_2) + B_1(z_1, z_2)] [C_{10}(z_1, z_2) - C_{11}(z_1, z_2)], \\ DA_2''(z_1, z_2) &= \frac{1}{8} [A_0(z_1, z_2) + A_1(z_1, z_2)] [B_0(z_1, z_2) - B_1(z_1, z_2)] [C_{20}(z_1, z_2) + C_{21}(z_1, z_2)], \\ DA_3''(z_1, z_2) &= \frac{1}{8} [A_0(z_1, z_2) + A_1(z_1, z_2)] [B_0(z_1, z_2) - B_1(z_1, z_2)] [C_{20}(z_1, z_2) - C_{21}(z_1, z_2)], \\ DA_4''(z_1, z_2) &= \frac{1}{8} [A_0(z_1, z_2) - A_1(z_1, z_2)] [B_0(z_1, z_2) + B_1(z_1, z_2)] [C_{30}(z_1, z_2) + C_{31}(z_1, z_2)], \\ DA_5''(z_1, z_2) &= \frac{1}{8} [A_0(z_1, z_2) - A_1(z_1, z_2)] [B_0(z_1, z_2) + B_1(z_1, z_2)] [C_{30}(z_1, z_2) - C_{31}(z_1, z_2)], \\ DA_6''(z_1, z_2) &= \frac{1}{8} [A_0(z_1, z_2) - A_1(z_1, z_2)] [B_0(z_1, z_2) - B_1(z_1, z_2)] [C_{40}(z_1, z_2) + C_{41}(z_1, z_2)], \\ \text{and} \\ DA_7''(z_1, z_2) &= \frac{1}{8} [A_0(z_1, z_2) - A_1(z_1, z_2)] [B_0(z_1, z_2) - B_1(z_1, z_2)] [C_{40}(z_1, z_2) - C_{41}(z_1, z_2)] \end{aligned} \quad ..(25)$$

Finally, this directional decomposition stage is cascaded with the predesigned 2-D circular split scheme (CSS) to form the total structure of the proposed CCT and the output of the i^{th} band is given by

$$Y_i(z_1, z_2) = DA_i''(z_1, z_2) X(z_1, z_2) \quad \text{for } i = 0, 1, 2, \dots, 8. \quad (26)$$

where $X(z_1, z_2)$ is the scaled image from the CSS stage.

It can be seen that the resulting structure of Fig. 13 is a regular and a modular one. Such properties make it suitable for VLSI implementation.

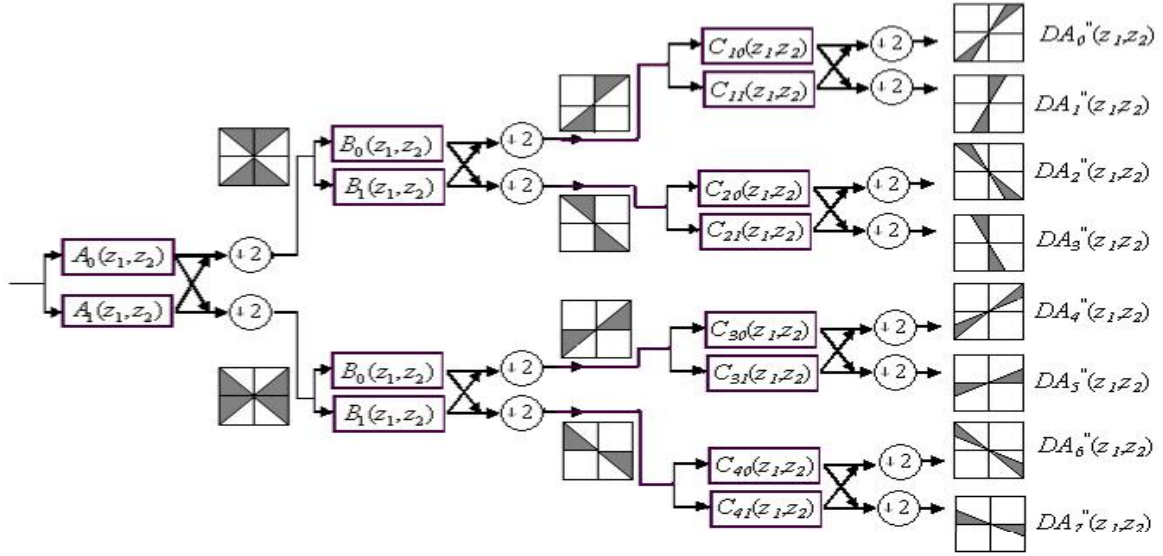


Fig. 13 8-band directionally-decomposed analysis bank

V. ASSESSMENT AND COMPARATIVE STUDY

In this section, the performance of the proposed CCT transform is evaluated and compared with that of the ordinary CT transform. A test image as the one shown in Fig. 14(a) is applied as an input to both CT & CCT transforms. The resulting directional details of the eight bands for both CT & CCT transforms are shown in Fig. 14(b). In such figure, it can be seen that due perfect circular and directional decompositions of high frequency bands in CCT, each band simulates the details in its direction with a better high-low frequency resolution because of using CSS instead of LP. This indicates the superiority of CCT in preserving image details. The objective performance of the proposed CCT transform is also evaluated via calculating an assessment parameter which is called *Deflection Ratio* (DR_i) at each directional band i , for $i = 0, 1, 2, \dots, 8$. DR_i is used here as a performance estimator. A proposed formula for this deflection is given by [15],[16]

$$DR_i = \frac{1}{R * C} \sum_{r,c} \left(\frac{d_i(r,c) - MV_i}{SD_i} \right) \quad (27)$$

where $d_i(r,c)$ represents the i^{th} detail image pixels of the i^{th} resulting CT or CCT bands, and $R * C$ is its size. Also

$$MV_i = \frac{\sum_{r,c} d_i(r,c)}{R * C} \quad (28)$$

and

$$SD_i = \sqrt{\frac{\sum_{r,c} [d_i(r,c) - MV_i]^2}{R * C}} \quad (29)$$

MV_i is the mean value with SD_i as the standard deviation, of the same i^{th} detail image pixels. It should be noted that, the ratio DR should be higher at pixels with stronger reflector points and lower elsewhere. Table-1 illustrates these DR_i values for different CT and CCT directional bands. From such table, the value of DR in each band of CT is modified in the case of CCT, referring to accurate definition of image details in that direction. It is believed that, the use of CSS instead of LP, is also the reason of such modifications. The previous properties nominate

the proposed CCT as a candidate instead of the classical CT to be utilized in those fields of image processing (such as denoising, compression and classification) which need better edge representations.

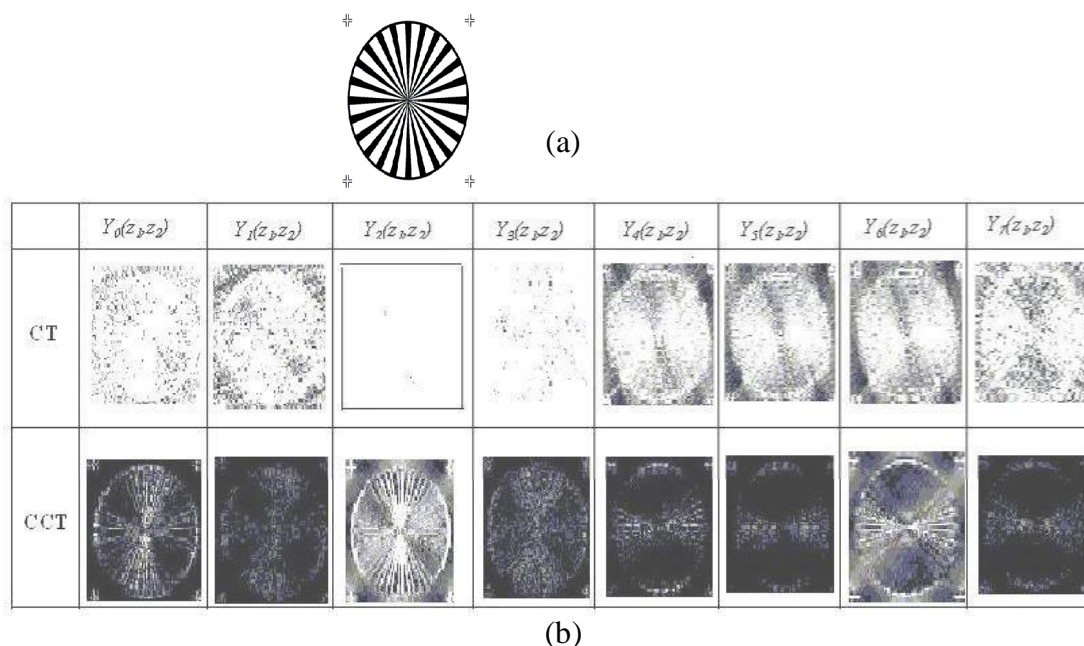


Fig. 14 (a) Original image, (b) It's directional details of the eight bands for both CT & CCT.

Table-1 Directional ratio DR_i values for different CT and CCT directional bands

DIRECTIONAL BAND i	0	1	2	3	4	5	6	7
DR_i WITH CT	9.01×10^{-4}	0.9179	0.0876	0.9118	0.0884	0.9114	0.0904	0.9093
DR_i WITH CCT	2.87×10^{-5}	0.8970	0.1031	0.8968	0.1032	0.8968	0.1033	0.8967

VI. CONCLUSIONS

A proposed circular contourlet transform based on both circularly- and directionally-support decomposition structures has been designed and realized utilizing lattice all-pass sections. The idea is based on using a circular-split scheme (CSS) followed by multiresolution DFB with many levels of decomposition. The proposed circular contourlet transform has been discussed and an execution algorithm has been adopted for the calculation of such transform. The details of a test image) has been analyzed via this circular contourlet transform. The resulting detailed images have been compared with the corresponding detailed images due to the application of the classical contourlet transform. From objective measures point of view, the resulting assessment parameter, Deflection Rate (DR) has indicated the superiority of such proposed CCT for perfect detail preservation. In addition to that, the resulting subband images from the proposed CCT are visually better where significantly more levels of detail are retrieved. The comparison also indicates that the application of the proposed circular contourlet transform results in more continuous contours (edges). On the other hand, from realization point of view, it is believed that the resulting structures preserve both modularity and regularity properties which are suitable for VLSI implementations. Besides, since such CCT is realized in a lattice all-pass sections, then some saving in computation can be gained,

while lattice structure will provide the system with a reduced sensitivity to finite word length effect.

REFERENCES

- [1] M. Antonini, M. Barlaud, P. Mathieu, and I. Daubechies, "Image compression using wavelet transform", *IEEE Trans. on Image Proc.*, Vol. 1, No, pp.205-220, April 1992.
- [2] M. Vetterli, J. Kovacevic, "Wavelets and subband coding", *Englewood Cliffs, NJ: Prentice Hall*, 1995.
- [3] S. Mallat, "A Wavelet Tour of Signal Processing", *Academic Press, New York*, 1998.
- [4] V. Velisavljevic, P. L. Dragotti, and M. Vetterli, " Directional wavelet transforms and frames", *Proc. IEEE Int. Conf. on Image Proc.*, 3:589-592, Sept. 2002.
- [5] M. N. Do and M. Vetterli, "Contourlets", *J. Stoeckler, G. V. Welland (Eds.), Beyond Wavelets*, pp.1-27, Academic Press, 2003.
- [6] M. N. Do and M. Vetterli, " The Contourlet transform: An efficient directional multiresolution image representation", *IEEE Trans. on Image Proc.*, Vol. 14, No. 12, pp. 2091-2106, Dec. 2005.
- [7] J. Rosiles and M. J. Smith, " Image denoising using directional filter banks", *Proc. IEEE Int. Conf. Image Proc.-2000*, pp. 292-295, 2000.
- [8] M. N. Do, "Directional multiresolution image representations", *Ph. D. thesis, EPFL, Lausanne, Switzerland*, Dec. 2001. on <http://www.ifp.uiuc.edu/~minhdo/publications/thesis.pdf>.
- [9] T. T. Nguyen and S. Orintara, " A multiresolution directional filter banks for image applications," *Proc. Int. Conf. Acoust., Speech & Signal Proc.*, Montreal, QC, Canada, May 2004.
- [10] T. T. Nguyen, " Multiresolution direction filter banks: Theory, design and applications" *IEEE Trans. on signal proc.*, Vol.53, No. 10, Oct. 2005.
- [11] B. A. Taha, " Directional wavelets; theory , design and application", *Ph. D. Thesis submitted to the college of Science, Dept. of Mathematics, University of Basrah*, Nov. 2007.
- [12] J. M. Abdul-Jabbar, "Design procedure of two-dimensional digital filter and filter bank," *Ph. D. Thesis submitted to the college of Eng. , Dept. of Elect. Eng., University of Basrah*, Sept. 1997.
- [13] S. Park, M. J. Smith, and R. M. Mersereau, "Improved structures of maximally decimated directional filter banks for spatial image analysis," *IEEE Trans. on image proc.*, Vol. 13, No. 11, pp. 1424-1431, Nov. 2004.
- [14] A. N. Willson and H. J. Orchard, "Insights into digital filters made as The sum of two allpass functions ," *IEEE Trans. Circuits Syst. -I: fundamental theory and applications*, Vol. 42, No. 3, pp. 129-136, Mar.1995.
- [15] M. Mastriani and A. E. Giraldez, " Kalman's Shrinkage for Wavelet-Based De-speckling of SAR Images", *International Journal Of Intelligent Technology*, Vol. 1, No. 3, pp. 190-196, 2006.
- [16] M. Mastriani, A. E. Giraldez, " Smoothing of coefficients in wavelet domain for speckle reduction in Synthetic Aperture Radar images", *The International Congress for Global Science and Technology (ICGST), International Journal on Graphics, Vision and Image Processing (GVIP), GVIP Special Issue on Denoising*, pp.1-8, 2007. on www.icgst.com

The work was carried out at the University of Mosul